Fragmentation spectra induced by light ions colliding with light nuclei

Th. Delbar, Gh. Grégoire, and P. Belery
Institut de Physique, Université Catholique de Louvain B-1348 Louvain-la-Neuve, Belgium

G. Paić
Institut Rudjer Bošković, PP 1016 Zagreb, Yugoslavia
(Received 21 June 1982)

Inclusive energy spectra of light charged particles from the ^{6}Li + ^{3}He, ^{9}Be+p, and ^{9}Be + ^{3}He reactions have been measured using beams of 30 to 75 MeV. The continuum parts have been studied in the framework of phase space calculations. The influence of other reaction mechanisms, such as final state interactions, sequential processes, and quasifree reactions is evaluated. We deduce the nontrivial angular dependence of the various phase spaces.

[NUCLEAR REACTIONS ^{6}Li + ^{3}He at E_{lab}=40 MeV; ^{9}Be + p at E_{lab}=45 MeV; ^{9}Be + ^{3}He, E_{lab}=30, 50, 75 MeV; measured charged light particle spectra $1 \leq Z \leq 4$, $1 \leq A \leq 9$; interpretation of inclusive spectra with phase space model; comparison with other models; deduced angular dependence of various exit channels.]

I. INTRODUCTION

A steady feature of particle energy spectra in nuclear reactions is a continuum part that escapes a full interpretation in terms of final state interaction or other peripheral mechanisms like quasifree scattering or transfer reactions to resonant states. However, the wealth of information about nucleon-nucleon forces and resonant states available through the study of the peripheral mechanisms has suppressed the interest for the study of the featureless continuum. In this framework the continuum part of the energy spectrum is generally considered as a background contribution apparently unrelated to the processes under study, and its shape is sometimes taken arbitrarily[1,2] or sometimes assimilated to the shape of one or more phase space distributions.[3] Some interest has emerged recently for the study of the main characteristics of the featureless part of the particle energy spectra.[3,4] To a certain extent this interest is connected with the efforts in heavy ion physics to gain insight into the succession of different collision processes.[5] On the contrary, in light systems the situation is far less complicated than in heavy systems so that more fundamental information may be obtained. Also, the precise determination of the parameters of nuclear resonances implies the best possible knowledge of the underlying continuum whenever such states are studied via nuclear reactions.

Concurrently with a recent study of the inclusive spectra of protons and deuterons emitted in $\alpha+\alpha$ collisions[4] we have undertaken a similar study using protons and ^{3}He projectiles on beryllium and lithium targets. We present here the data on the continuous part of the spectra, while the study of the parameters of the ^{6}Li levels is reported elsewhere.[6]

II. EXPERIMENT

The reactions reported in Table I were investigated using proton and ^{3}He beams from the variable energy cyclotron CYCLONE of the University of Louvain. For all reactions except ^{9}Be(p,α) at 75 MeV an analyzed beam was used.

We used two self-supporting beryllium targets (2.3 mg/cm^2 for the runs at 75 MeV and 380 μg/cm^2 thick for all other runs). The ^{6}Li targets were produced in the scattering chamber itself. Their thickness was 400 μg/cm^2 of 99.4% isotopically pure ^{6}Li metal evaporated onto a gold backing of 170 μg/cm^2. To prevent oxidation of the target by the residual gases in the scattering chamber the target holder was surrounded with a copper cylinder cooled with liquid nitrogen. The copper cylinder had appropriate holes for the incident and outgoing particles.

The charged particles were detected by a conventional ΔE-E telescope with a veto counter behind the E counter to prevent the long range light particles from loading the analog-to-digital converters (ADC's). The thicknesses of the ΔE detectors fix

TABLE I. Experimental conditions and threshold energies.

Reaction	Incident energy (MeV)	θ_{lab} (deg)	E_{min} (MeV)
^{6}Li(^{3}He,t)	40	10, 20, 30, 40	9.5
^{9}Be(^{3}He,^{6}He)	45	10, 20, 30	5.0
^{9}Be(^{3}He,^{6}Li)	45	10, 20, 30	9.0
^{9}Be(^{3}He,^{7}Li)	45	10, 20, 30	10.0
^{9}Be(^{3}He,^{7}Be)	45	10, 20, 30	13.0
^{9}Be(p,α)	75	10, 15, 20, 30, 40	24
^{9}Be(p,α)	50	10, 15, 20, 25, 30, 40, 50, 60, 90	13
^{9}Be(p,α)	30	10, 20, 25, 30, 35, 40, 50, 60	4.5

our threshold energies reported in the last column of Table I. The solid angle was 7.0×10^{-5} sr and the angular aperture was 0.3 deg. An additional detector placed at a fixed angle was used as a monitor for possible target deterioration.

Particle identification was achieved with a conventional Goulding circuit[7] for the measurement of the ^{9}Be(p,α) reaction at 75 MeV. In all other cases the E and ΔE information was recorded in a 4096×4096 array and stored on magnetic tapes for off-line analysis.

The identification was then made by drawing separation curves in the two-dimensional ΔE-E plot. The separation between α and ^{3}He particles was such that less than 0.04% of ^{3}He events could be counted as alphas. For the other detected charged particles the separation was of similar quality.

The energy calibration of the E and ΔE detectors for a given particle was made using the position of the peaks belonging to known discrete levels in all the spectra of that particle. Corrections for target thicknesses were made, providing finally a calibration error of about 0.1% in both E and ΔE channels.

The standard electronics was completed with antipileup units in the E- and ΔE-pulse lines. A pulse generator simulated ΔE-E events in a part of the spectrum free of actual events. It allowed dead time corrections and checked the performance of the electronics.

III. THEORETICAL CONSIDERATIONS

A. General

The first order perturbation theory gives for the differential cross section

$$\sigma=\frac{2\pi\,|\,T_{if}\,|^{2}}{\hbar\,|\,\text{flux}\,|}w\ , \tag{1}$$

where w is the density of states or phase space allowed by the conservations of energy and momentum.

In the case of a reaction giving N particles in the final state w takes the form

$$w=\frac{1}{(2\pi)^{3N}}\delta\left[\vec{k}_0-\sum_{i=1}^{N}\vec{k}_i\right]\delta\left[T_0-\sum_{i=1}^{N}T_i\right], \tag{2}$$

where $\vec{k}_0$ and T_0 are, respectively, the total wave number and the total kinetic energy to be shared between the N particles, and k_i and T_i are the wave number and kinetic energy of particle i.

If one out of the N particles is detected in a reaction $A(a,m_N)m_1,m_2,\ldots,m_{N-1}$ the inclusive spectrum takes the form

$$\frac{d^{2}\sigma}{d\Omega_N dT_N}=\frac{2\pi p_N m_N}{v_0\hbar^{4}}\int\cdots\int\prod_{i=1}^{N-1}\frac{d\vec{k}_i}{(2\pi)^{3}}\,|\,T_{if}\,|^{2}\delta\left[\vec{k}_0-\sum_{i=1}^{N}\vec{k}_i\right]\delta\left[T_0-\sum_{i=1}^{N}T_i\right], \tag{3}$$

where Ω_N, T_N, and p_N are the detection solid angle, the kinetic energy, and the momentum of the detected particle N; v_0 (p_0) is the velocity (momentum) of the incident particle; and T_{if} is the matrix element for the transition from the initial state i to a final state f.

$|\,T_{if}\,|^{2}$ may have two different behaviors with respect to its dependence on the momenta of the N particles:

(i) $|\,T_{if}\,|^{2}$ is not dependent or only slowly dependent on the momenta. In this case we have a situation corresponding to the so-called phase space model (PSM) first suggested by Fermi.[8]

(ii) $|\,T_{if}\,|^{2}$ is strongly dependent on the relative momenta of two or more particles in the final state. For such cases, in the absence of exact treatments of

many-body systems we distinguish several models appropriate to particular situations[9]: sequential decay (applied to resonant states in the continuum); final state interaction (applied to virtual levels in the continuum); and quasi-free scattering (or reaction), where a part of the system has a very low momentum and can be treated as a spectator to a scattering (or reaction) process between the incident particle and the remainder of the system.

B. Phase space model (PSM)

Fermi[8] proposed to replace $|T_{\rm if}|^2$ by a mean value C if a statistical equilibrium is reached. This is the so-called phase space model (PSM) or statistical model. The energy spectrum of the detected particle is given by

$$\frac{d^2\sigma}{d\Omega_N dT_N}=\frac{2\pi p_N m_N}{v_0\hbar^4}C \times R_{N-1}(m_1,\ldots,m_{N-1};T^*,P^*) , \tag{4}$$

where

$$T^*=T_0-T_N , \tag{5}$$

$$\vec{\mathrm{P}}^*=\vec{\mathrm{p}}_0-\vec{\mathrm{p}}_N , \tag{6}$$

and R_{N-1} is the phase space factor for the $N-1$ undetected particles

$$R_{N-1}=D_{N-1}\left[T^*-\frac{P^{*2}}{2\sum_{i=1}^{N-1}m_i}\right]^{(3N-8)/2} . \tag{7}$$

The Galilean invariant expression in brackets is the total kinetic energy of the $(N-1)$ undetected particles in their center of mass system. D_N has the form

$$D_N=\frac{1}{h^{3(N-1)}}\frac{(2\pi)^{3(N-3)/2}}{\Gamma(\frac{3}{2}(N-1))}\frac{\left[\prod_{i=1}^{N}m_i\right]^{3/2}}{\left[\sum_{i=1}^{N}m_i\right]^{3/2}} . \tag{8}$$

We remark that the dimensions of R_{N-1} change with the number of particles involved in the final state. Whenever the number of particles increases by one, the phase space is divided by a volume. This change of dimensions is compensated in the calculation of $|T_{if}|^2$. This can be understood by the requirement that the new particle be also included in the interaction volume, as suggested by Fermi.[8]

It should be noted that C is not a constant for the whole volume of the phase space.[10] C may depend on the momentum p_N, on the direction of the detected particle, and on the incident energy. In the present study we neglect the dependence on p_N but allow for a dependence on the angle of emission, an assumption supported *a posteriori* by our results and tacitly assumed by all authors using the phase space model (e.g., Refs. 3 and 11).

Equation (7) is strictly valid only for cases where the total angular momentum L of the system is zero. This point has been discussed by Delves[12] and Cerulus.[13] Cerulus claims that for $L=1$ or 2 the shape of the spectrum should not be very different from the $L=0$ case. In our calculations we neglected the conservation of angular momentum and the spins of the particles.

C. Sequential processes

Two situations may occur when measuring the spectrum of particle b emitted after a reaction $A+a\rightarrow b+B+c$ in the presence of a two-body resonance.

(i) Particle b does not belong to the resonant pair. In this case the energy spectrum of b has a one-to-one correspondence with the excitation energy of the B-c system.

(ii) Particle b belongs to the resonant pair. The expected spectral shape was calculated by Morinigo.[14]

D. Final state interaction

We used the Jost enhancement factor given by Watson[15] to take into account a final state interaction between two nucleons:

$$F_j=\frac{(k^2+\alpha^2)\frac{r_e}{2}}{-\frac{1}{a}+\frac{r_e k^2}{2}-ik} , \tag{9}$$

where k is the relative wave number, a is the scattering length, and r_e is the effective range for the two-nucleon system under consideration,

$$\alpha=\frac{1}{r_e}\left[1+\left[1-\frac{2r_e}{a}\right]^{1/2}\right] . \tag{10}$$

E. Quasi-free scattering $A(a,b)ac$

The detection of the scattered part of the target nucleus may lead to enhancements in the spectra. In an inclusive experiment we integrate over the directions of the scattered particle a. If the scattering takes place between a and b the energy spectrum of particle b is given by the expression

$$\frac{d^2\sigma}{d\Omega_b dT_b}=\frac{(m_a+m_b)^2}{(2\pi)^3\hbar^2 k_0 m_b}k_b \times\int d\Omega_a\left[\frac{d\sigma_{ab}}{d\Omega}\right]_{\text{c.m.}} k_a\frac{1}{f}P(q)\ , \tag{11}$$

where

$$f=1+\frac{m_a}{m_b}\left[1-\frac{k_0}{k_a}\cos\theta_{0a}+\frac{k_b}{k_a}\cos\theta_{ab}\right]\ , \tag{12}$$

k_0, k_a, and k_b are the wave numbers of particle a before scattering, of particle a after scattering, and of particle b, respectively; θ_{0a} is the scattering angle of particle a; θ_{ab} is the angle between particles a and b after the collision; $P(q)$ is the momentum distribution of b in the target nucleus; and

$$\left[\frac{d\sigma_{ab}}{d\Omega}\right]_{\text{c.m.}}$$

is the differential cross section for the elastic scattering of a on b in the post form.[16]

IV. DATA ANALYSIS

For the given target, incident energy, and detected particle we construct an incoherent sum of energy spectra given by Eq. (4) for a particular channel, namely,

$$\frac{d^2\sigma}{d\Omega_N dT_N}=\frac{2\pi p_N m_N}{v_0\hbar^4}\sum_i C_i R_{N-1}^{(i)}(m_1^{(i)},m_2^{(i)},\ldots,m_{N-1}^{(i)};T^{*(i)},P^*)\ , \tag{13}$$

where the index i refers to the ith breakup channel.

In our fits to the data the number of breakup channels and the strength coefficients C_i were the only free parameters. The convolution of expression (13) with a Gaussian energy resolution function is corrected for energy losses in the target before comparison to the data. The C_i coefficients were obtained with a least squares method using those parts of the energy spectra assumed to be free of contributions from discrete states in the exit channel.

The energy scale shown in the figures for the detected particles refers to the energy in the detector. The corrections for energy losses in the target were introduced at every point in the fits assuming that all particles emerge from the center of the target. Since the correction used is not completely valid below our threshold energy, the fits do not always reach zero value at zero energy as they theoretically should. In some cases it was found necessary to include ^{5}He and/or ^{5}Li contributions in the fits. Care was then taken to smear out the corresponding theoretical phase space spectrum for the width of the ground state of the unstable particle.

V. RESULTS

The number of exit channels in the fitting procedure was set to a minimum as long as the chi square remained unaltered by the truncation. If two mirror channels were involved, e.g., for the ^{9}Be(p,α) reaction when the undetected particles are $(n,^5\text{Li})$ and $(p,^5\text{He})$ or similarly $(^3\text{He},d,n)$ and (t,d,p), we took only one of them on the basis of the almost identical Q values and shapes of the spectra for the mirror channels.

We use two ways to show the relative importance of individual final channels:

(i) We tabulate the strength coefficients C_i. They represent the average value of the squares of the matrix elements involved in Eq. (13). They are given in $(\text{MeV}^2(\text{fm})^{3N})$.

(ii) We tabulate the ratio of individual phase space contributions (weights) to the total spectrum at a given angle

$$x_i=\frac{(d\sigma/d\Omega_N)_i}{\sum_i (d\sigma/d\Omega_N)_i}\ . \tag{14}$$

To compute this ratio, an extrapolation is carried out below the experimental threshold energy, neglecting the contributions of channels that open below it. One should bear in mind that angular distributions of $(d\sigma/d\Omega)_i$ or x_i are misleading, since they hide angle-dependent kinematical factors, the matrix elements or the strength coefficients C_i being constant. This effect is illustrated in Fig. 1.

The errors quoted for C_i are purely statistical (one standard deviation) and they contribute as such in computing the χ^2 value per data point. It should be stressed that in all cases the χ^2 value per data point was always less than 1.45, the average value being (1.11 ± 0.16). This gives an estimate of the good quality of the fits. All spectra are presented in the laboratory frame.

A. ^{6}Li(^{3}He,t) reaction

A representative spectrum with the corresponding PSM fit is shown in Fig. 2. The analysis has shown

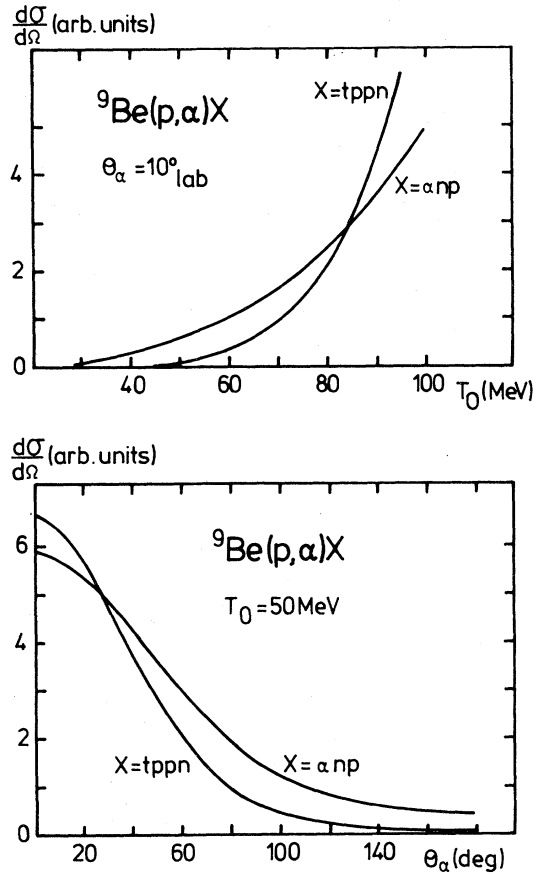

FIG. 1. Phase space model differential cross section for the ^{9}Be(p,α) reaction, with a constant matrix element as a function of the incident energy (upper part) and of the detection angle (lower part).

that only two phase spaces are sufficient to fit the data at all angles. The extracted C_i's and weights x_i are given in Table II. The strength coefficient for the t^5Lip channel decreases smoothly with angle, whereas for the $t\alpha pp$ final state it peaks around 30°. In a different context this behavior would be typical of a direct reaction mechanism, but in the present case more data points would be needed (especially at larger angle) to support this analogy.

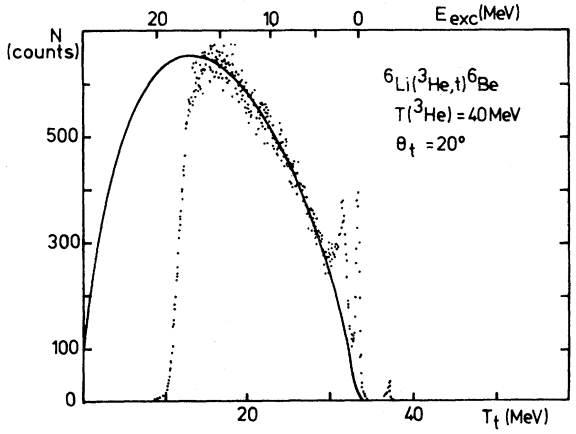

FIG. 2. Experimental spectrum for the reaction ^{6}Li(^{3}He,t) at $T(^3\text{He})=40$ MeV and $\theta_t=20°$. The continuous line is the PSM fit.

B. ^{9}Be(^{3}He,^{6}He) and ^{9}Be(^{3}He,^{6}Li) reactions

Spectra at 20° are shown in Fig. 3. The extracted strength coefficients and weights are given in Table III. The strength coefficients for the ^{9}Be(^{3}He,^{6}Li) reaction were calculated neglecting the contribution of the ^{9}Be(^{3}He,^{6}Li$_{3.56\ \text{MeV}}$) reaction. Should this reaction play a noticeable role, one should find in the spectrum discrete peaks due to it. The fits for these reactions required three phase spaces.

Comparing the spectra and coefficients for the ^{6}Li(^{3}He,t) and ^{9}Be(^{3}He,^{6}He) reactions leading to the same residual particles we observe the following:

(i) The ground state and 1.67 MeV level in ^{6}Be are populated by the (^{3}He,t) charge exchange reaction, whereas they are not seen with the (^{3}He,^{6}He) reaction. This agrees with the predicted cluster structure of the targets.

(ii) The dominant contributions to the continuum spectrum are also different for the two reactions.

As far as the ^{9}Be(^{3}He,^{6}Li) case is concerned, three contributions (^{6}Liαd, ^{6}Liαnp, and ^{6}Litdp) almost totally exhaust the measured cross section. There is some similarity with the results obtained for the

TABLE II. The ^{6}Li(^{3}He,t) reaction at $T(^3\text{He})=40$ MeV. Strength coefficients C (arbitrary units), weights X of individual exit channels.

Reaction	θ_{lab} (deg)	10°	20°	30°	40°
^{6}Li(^{3}He,t)^{5}Lip	C	40.9±0.4	15.8±0.2	13.4±0.3	11.0±0.2
	X	1.0	0.70	0.49	0.97
^{6}Li(^{3}He,t)αpp	$10^{-1}C$	0.0±1.4	27.8±1.0	59.7±1.4	1.7±1.2
	X	0	0.30	0.51	0.03

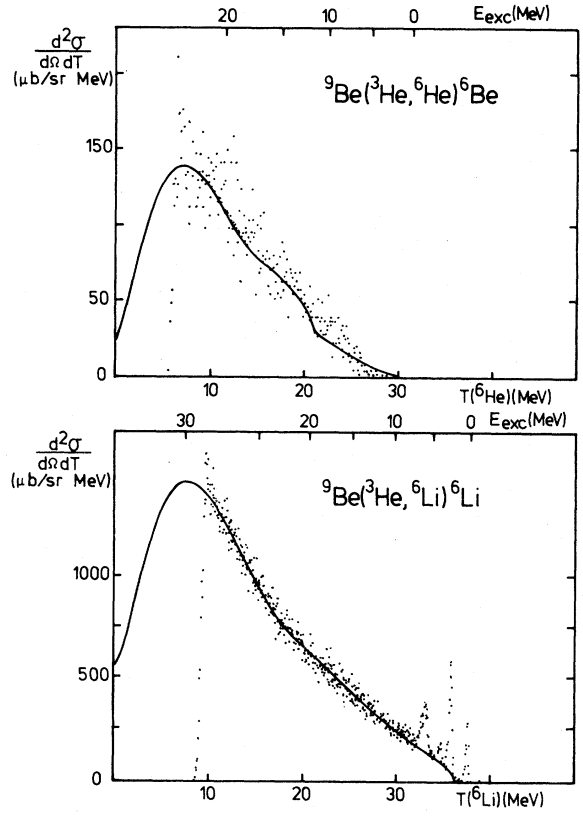

FIG. 3. Experimental spectra taken at $T(^3\text{He})=45$ MeV and $\theta=20°$ for the reactions ^{9}Be(^{3}He,^{6}He)^{6}Be (upper part) and ^{9}Be(^{3}He,^{6}Li)^{6}Li (lower part). The continuous lines are the PSM fits.

^{9}Be(^{3}He,^{6}He) reaction, except for the absence of the (^{6}Lit^3He) channel.

Although the statistical equilibrium approach inherent to the phase space model predicts independence from entrance channel effects, such effects do emerge from the experiment.

C. ^{9}Be(^{3}He,^{7}Li) and ^{9}Be(^{3}He,^{7}Be) reactions

Spectra at 20° are shown in Fig. 4. The coefficients and weights are given in Table IV. The fits were made in the region corresponding to $E_x(^5\text{Li})$ or $E_x(^5\text{He})>13$ MeV due to the presence of known states. The fit at 10° in ^{9}Be(^{3}He,^{7}Li) is somewhat poorer ($X^2=1.42$) than at 20° and 30° because of the contribution of the very broad first excited level of the ^{5}Li nucleus, whose energy and width are very poorly known[17] ($E_x=5-10$ MeV, $\Gamma=5\pm2$ MeV).

The comparison of the ^{7}Li and ^{7}Be spectra yields the following information:

(i) Almost no excitation of the ground state of ^{5}Li nucleus is seen in the ^{7}Li spectrum, while the ^{7}Be spectrum exhibits a strong peak corresponding to the ^{5}He ground state. This difference in the spectra is in agreement with the strong α-^{5}He clustering of ^{9}Be.

(ii) The ^{9}Be cluster structure also manifests itself in the continuum spectra, where a smaller weight is observed for the ^{7}Li-α-p continuum than for the ^{7}Be-α-n continuum.

TABLE III. The ^{9}Be(^{3}He,^{6}He) and ^{9}Be(^{3}He,^{6}Li) reactions at $T(^3\text{He})=45$ MeV. Strength coefficients C (in MeV^2 fm^{3N}), where N is the number of outgoing particles), weights X of individual exit channels.

Reaction	θ_{lab} (deg)	10°	20°	30°
^{9}Be(^{3}He,^{6}He)αpp	$10^{-10}C$	2.35±0.69	2.29±0.28	3.12±0.22
	X	0.48	0.56	0.69
^{9}Be(^{3}He,^{6}He)^{3}He^{3}He	$10^{-7}C$	6.7 ±2.0	4.9 ±1.0	2.2 ±0.9
	X	0.24	0.21	0.10
^{9}Be(^{3}He,^{6}He)^{3}Hedp	$10^{-11}C$	2.44±0.26	2.25±0.26	4.23±0.52
	X	0.28	0.23	0.21
^{9}Be(^{3}He,^{6}Li)αd	$10^{-8}C$	7.12±2.56	4.47±0.89	2.93±0.68
	X	0.24	0.21	0.17
^{9}Be(^{3}He,^{6}Li)^{5}Hep	$10^{-8}C$	0.0 ±6.3	1.7 ±2.1	0.74±1.52
	X	0	0.04	0.02
^{9}Be(^{3}He,^{6}Li)αnp	$10^{-11}C$	5.42±0.60	3.96±0.23	4.08±0.16
	X	0.51	0.49	0.57
^{9}Be(^{3}He,^{6}Li)tdp	$10^{-11}C$	20.3 ±2.1	16.8 ±1.2	23.0 ±1.6
	X	0.25	0.23	0.24
^{9}Be(^{3}He,^{6}Li)$tppn$	$10^{-15}C$	0.0 ±5.0	7.6 ±6.4	0. ±45.
	X	0	0.03	0

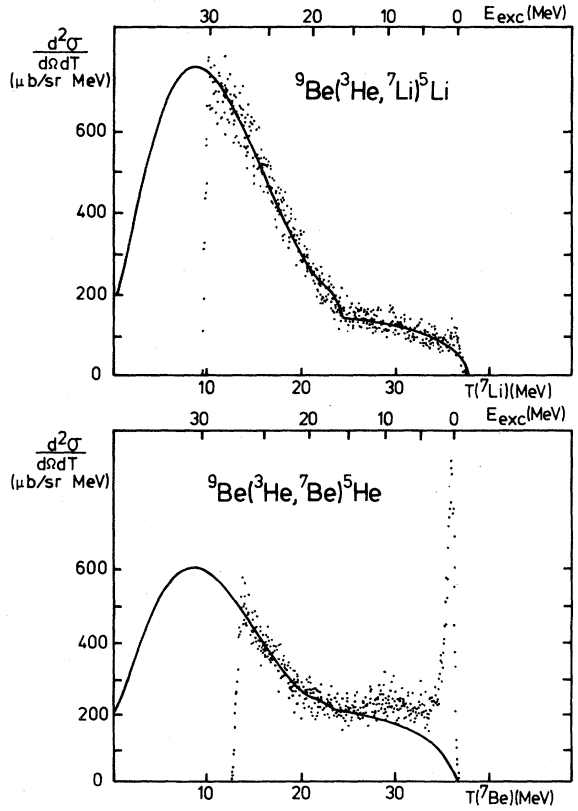

FIG. 4. Same conditions as Fig. 3 for the reactions ^{9}Be(^{3}He,^{7}Li)^{5}Li (upper part) and ^{9}Be(^{3}He,^{7}Be)^{5}He (lower part).

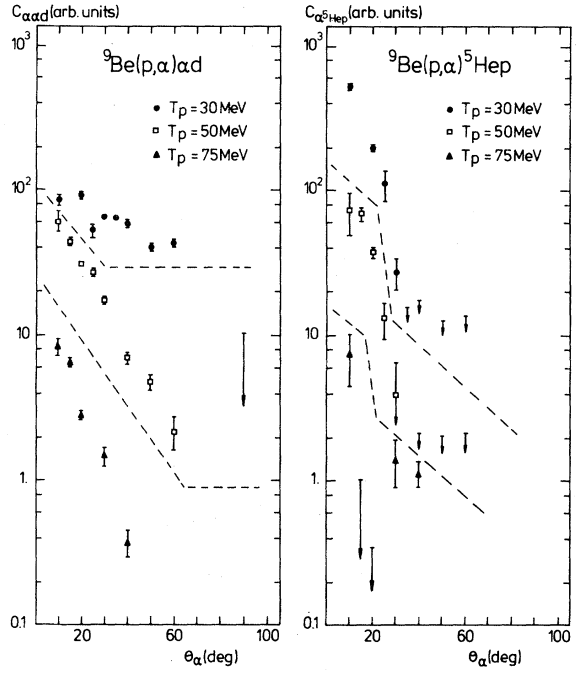

FIG. 5. Angular distributions of the $(\alpha\alpha d)$ and $(\alpha^5 He p)$ strength coefficients for the reaction ^{9}Be(p,α) at $T_p=30$, 50, and 75 MeV.

D. ^{9}Be(p,α) reaction

This reaction was studied at 30, 50, and 75 MeV incident proton energy and the results were always analyzed using the same minimum set of phase spaces. A small carbon contamination was seen at 30 and 50 MeV around $E_x(^6\text{Li})\sim 8$ MeV. The angular distributions of the strength coefficients are shown in Figs. 5–7.

1. $T_p=75$ MeV

Spectra at 15° and 20° are shown in Fig. 8. The α^3Het phase space contribution occurring above

TABLE IV. Same as Table III for the ^{9}Be(^{3}He,^{7}Li) and ^{9}Be(^{3}He,^{7}Be) reactions at $T(^3\text{He})=45$ MeV.

Exit channel	θ_{lab} (deg)		10°	20°	30°
^{9}Be(^{3}He,^{7}Li)αp		$10^{-8}C$	6.66±0.14	4.99±0.07	4.80±0.05
		X	0.30	0.32	0.36
^{9}Be(^{3}He,^{7}Li)^{3}Hed		$10^{-8}C$	6.60±0.27	4.70±0.16	4.57±0.15
		X	0.21	0.20	0.20
^{9}Be(^{3}He,^{7}Li)^{3}Hepn		$10^{-11}C$	14.04±0.25	12.47±0.21	14.31±0.38
		X	0.49	0.48	0.44
^{9}Be(^{3}He,^{7}Be)αn		$10^{-8}C$	11.93±0.47	7.61±0.16	5.84±0.36
		X	0.55	0.52	0.45
^{9}Be(^{3}He,^{7}Be)td		$10^{-8}C$	3.92±0.72	1.65±0.29	4.20±0.63
		X	0.13	0.07	0.19
^{9}Be(^{3}He,^{7}Be)tpn		$10^{-11}C$	10.20±0.65	11.15±0.51	13.00±1.71
		X	0.32	0.41	0.36

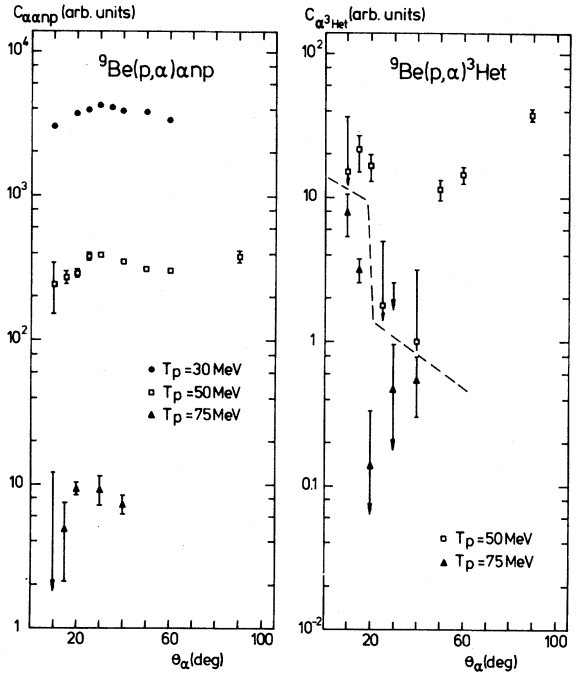

FIG. 6. Same as Fig. 5 for the ($\alpha\alpha np$) and (α^3Het) final states.

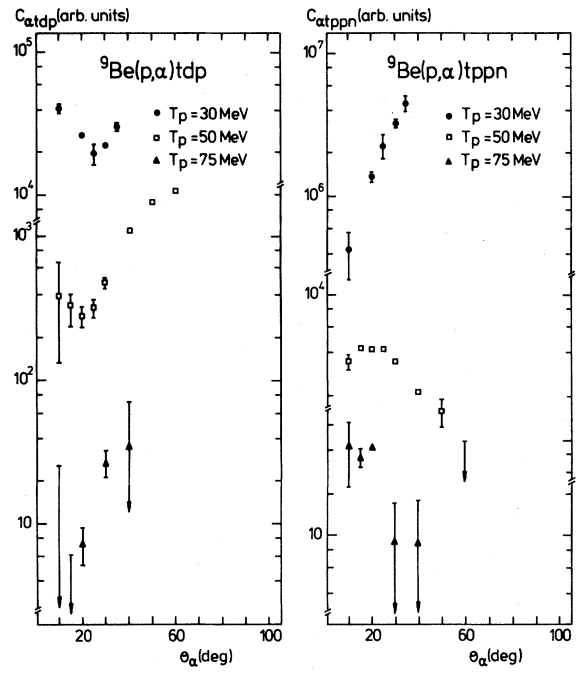

FIG. 7. Same as Fig. 5 for the (αtdp) and ($\alpha tppn$) final states.

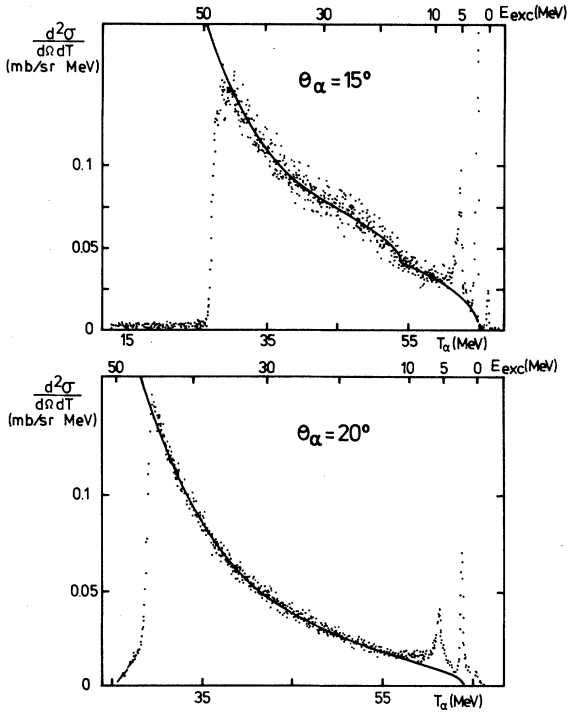

FIG. 8. Experimental spectra of the reaction ^{9}Be(p,α) at $T_p=75$ MeV and $\theta_\alpha=15°$ (upper part), 20° (lower part). The continuous lines are the PSM fits.

$E_x=15$ MeV is clearly seen at 15° but vanishes at 20°.

2. $T_p=50$ MeV

Spectra at 20° and 50° are shown in Fig. 9. For angles larger than 40°, the discrepancy in the excitation energy interval 15–25 MeV is not removed when one uses a complete set of phase spaces.

3. $T_p=30$ MeV

A spectrum taken at 30 deg is shown in Fig. 10. At 30 MeV the spectra exhibit a marked change in the slope of the continuum at $E_x(^6\text{Li})=13$ MeV. The fits were done in the region of equivalent ^{6}Li excitation energy from 13 to 18 MeV and above 24 MeV, when allowed by our threshold energy (i.e., at small angles). The region 18–24 MeV was excluded due to the existence of known states of ^{6}Li.[17] In fact, these levels were not observed at other measured energies.

4. Discussion of the ^{9}Be(p,α) results

The spectra at all energies present a departure from a smooth continuum behavior in the part of the spectra corresponding to a 6–12 MeV excitation

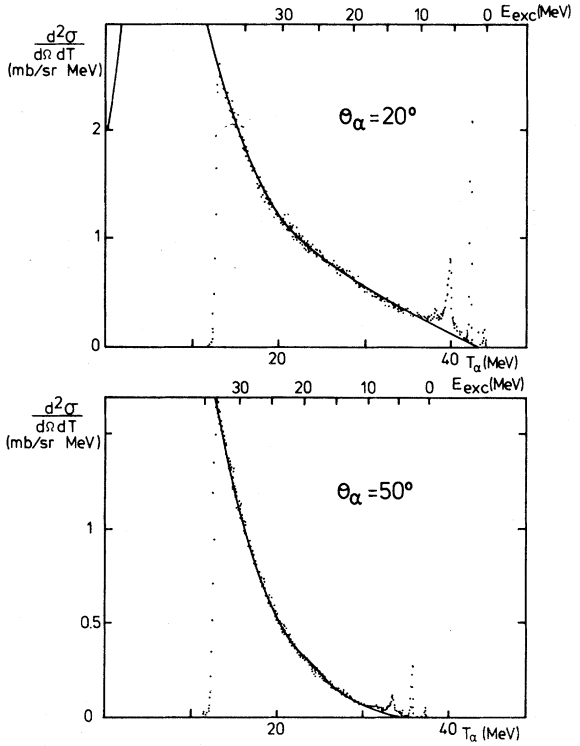

FIG. 9. Same as Fig. 8 at $T_p = 50$ MeV and $\theta_\alpha = 20°$ (upper part) and 50° (lower part).

of ^{6}Li. This feature could not be satisfactorily explained by any set of phase spaces. We attempted to explain it by adding contributions from the following processes:

(i) p-α quasi-free scattering using relation (11). The (p,α) scattering cross sections were taken from published data.[17,18] The momentum distribution for the α particle in ^{9}Be had a Gaussian shape with a FWHM of 120 MeV/c.[19] The contribution of this process at $T_p = 30$ MeV is shown in Fig. 11 assuming a ^{5}He spectator. Both in shape and in magnitude the quasi-free process cannot explain the observed anomaly.

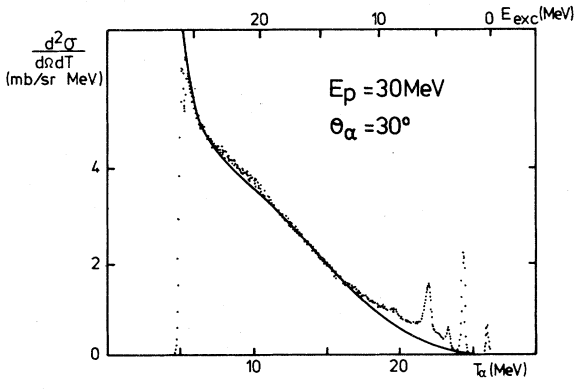

FIG. 10. Same as Fig. 8 at $T_p = 30$ MeV and $\theta_\alpha = 30°$.

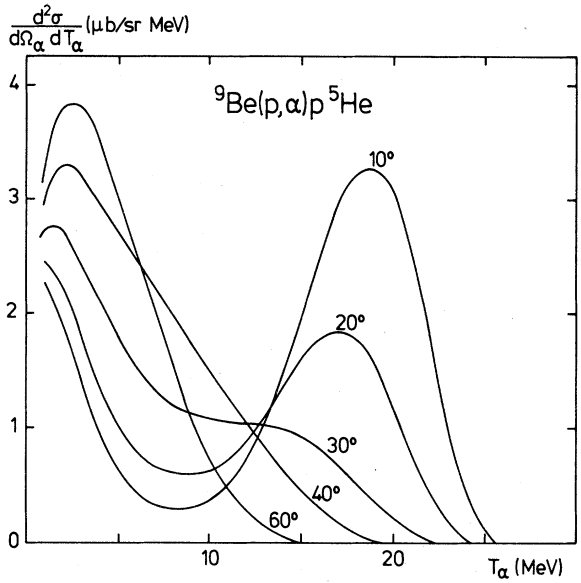

FIG. 11. Calculated spectra of the PWIA quasi-free scattering contribution for the ^{9}Be$(p,\alpha)p^5$He reaction at $T_p = 30$ MeV and $\theta_\alpha = 10°$, 20°, 30°, 40°, and 60°.

(ii) The contribution of the final state interaction (FSI) of a n-p pair has been calculated using the method explained in Sec. III D. The final channel was of the form $\alpha\alpha(np)$, i.e., with an interacting neutron-proton pair and no interaction between the other clusters. The shapes of the spectra calculated for n-p singlet and triplet interactions are very similar to the $(\alpha\alpha np)$ phase space (Fig. 12). The presence of FSI cannot explain the discontinuity in the continuum spectrum observed at $E_x(^6\text{Li}) \sim 13$ MeV.

(iii) The possibility of detecting an alpha particle belonging to a resonance in the sense explained in Sec. III C was investigated using the relation of Morinigo.[14] All possible resonances that can be reached from a $p + {}^9$Be entrance channel have been tested to explain the anomaly at $E_x(^6\text{Li}) \sim 6$–12 MeV. The results of this investigation also proved to be fruitless in explaining the shape of the spectra.

The only alternative left is the presence of a broad resonance (or resonances) in the ^{6}Li nucleus as suggested by one of our earlier measurements.[20] To support this assumption we should add that the observed anomaly follows the kinematics of a ^{6}Li level and is seen in the ^{9}Be(^{3}He,^{6}Li) spectrum at 10°.

All the approaches described above have also been attempted to explain the departure of the fits from the observed spectra at $E_x(^6\text{Li}) \sim 18$–24 MeV and $E_p = 30$ MeV. Here also the only explanation left is

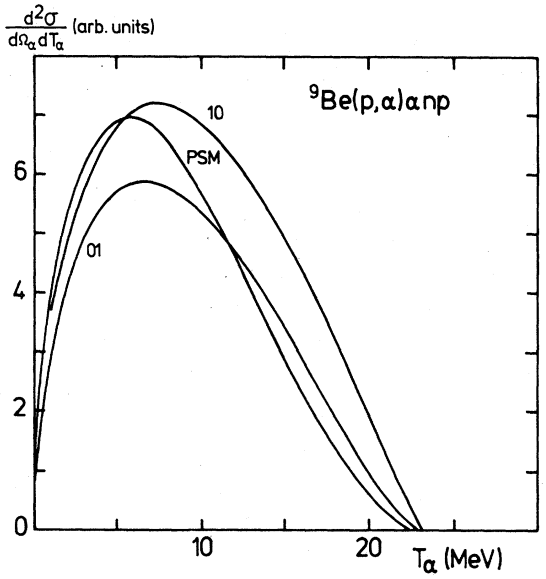

FIG. 12. Influence of a n-p final state interaction for the ^{9}Be(p,α)αnp reaction at $T_p=30$ MeV, $\theta_\alpha=30°$. The curve labeled PSM is the pure phase space model prediction. The lines labeled (10) and (01) refer to the addition of a singlet and triplet n-p interaction, respectively.

the existence of broad levels as suggested by the phase shift analysis[21] of the ^{3}He + t elastic scattering.

The coefficients decrease with increasing incident energy. One could explain this behavior by the increasing number of channels opening with energy. It is expected that at higher energy, but below the pion threshold, this behavior would almost disappear when all channels would be open. For instance, the data obtained in the case of the $\alpha+\alpha$ reaction[4] after removing the kinematical factors seem to support this idea. However, there are clearly distinct trends depending on the number of particles in the exit channel. The three body channels generally fall off very rapidly with increasing angle, while the four body contributions stay approximately constant with angle.

VI. CONCLUSION

Our experiments demonstrate that an important part of the interaction between incident light particles (protons and ^{3}He) and a light target nucleus (lithium and beryllium) results in a continuum spectrum. It does not agree with interpretations in terms of conventional models like stripping and pickup to resonant states, quasi-free scattering, and final state interactions. We have successfully applied a phase space model whose main characteristics are the following:

(i) A statistical equilibrium between all outgoing particles is reached during the interaction.

(ii) The interaction is supposed to be independent of the momenta of the outgoing particles.

(iii) Angular momentum conservation is not taken into consideration.

(iv) The experimental spectrum is represented by an incoherent sum of several allowed exit channels weighted by strength coefficients (free parameters). We generally needed many fewer exit channels than the number of kinematically allowed ones. The dominant exit channels are closely correlated to the generally accepted cluster configuration involved in the entrance channel.

Overall good fits are achieved with spectra of very different reactions in a broad range of incident energies and in a large energy interval for the detected particles. Only the ^{9}Be(p,α) reaction above 40° gives less satisfactory fits.

The angular dependence of the strength coefficients and therefore the corresponding matrix elements for individual exit channels exhibit a different behavior for the three and four body exit channels. While the strength coefficients of the three body channels tend to decrease very rapidly with increasing detection angle, those of the four body channels stay approximately constant. On the other hand, the strength coefficients of individual exit channels decrease rapidly with increasing incident energy.

The features mentioned above invite the following comments:

(i) Entrance channel effects suggest that the statistical equilibrium is not reached.

(ii) The angular dependence of the strength coefficients, although unusual in a statistical equilibrium model, is, however, compatible with the predictions of the model as pointed out by Hagedorn.[10]

(iii) The dependence on incident energy is not surprising and may be attributed to the energy dependence of the interaction and/or to the opening of competing exit channels at higher energy.

(iv) The phase space model may show, in principle, a dependence on the momenta of the detected particles.[10] We do not observe such a dependence in the spectra measured at forward angles. It is, however, questionable whether the slightly inferior fits obtained for the ^{9}Be(p,α) reaction at angles above 40° should be taken as evidence for such a dependence.

(v) The good fits achieved without considering the angular momentum conservation can be understood if only low angular momenta are involved in the process.[13] Such a picture is attractive because the phase space model would be complementary to the usual treatment of peripheral two-body and quasi-

two-body processes[22] as far as angular momentum is concerned.

(vi) Our results show the power of the phase space model to detect otherwise almost indiscernible anomalies in the spectra due to broad resonances and/or quasi-free scattering. The subtraction of the phase space contribution enabled us to observe the known levels in ^{6}Li at $\sim$21 and 21.5 MeV that have not been detected so far in charged particle reactions. The low cross section for excitation of these levels prevented us from extracting their precise parameters. Similarly we have confirmed the existence of an anomaly in the region of $E_x(^6\text{Li})\sim 8-12$ MeV that might correspond to one or more resonances in ^{6}Li, as suggested in our earlier work.[20] It is important that this result has been obtained both from the ^{9}Be(^{3}He,^{6}Li) and the ^{9}Be(p,α) reaction. The spectra of the ^{6}Li(^{3}He,t) reaction do not indicate a similar anomaly in the corresponding excitation range for ^{6}Be. No definite conclusions on the isospin assignment can be drawn since the reaction mechanisms involved may be different.

(vii) The observed exit channels yield information on the cluster structure of the initial state. Contrary to the situation where the cluster structure is studied in transfer reactions or in quasi-free scattering, the phase space model yields information on the multiple cluster structure (i.e., when the number of clusters is larger than two).

Many features of the fragmentation spectra can be satisfactorily interpreted with the phase space model. It should encourage further theoretical studies on details not included here, like total angular momentum conservation, predictions of angular distributions, and energy dependence.

ACKNOWLEDGMENTS

The authors are deeply indebted to Mr. Jacques Bertrand for continuous help. One of us (P.B.) wishes to thank the "Institut pour la Recherche Scientifique dans l'Industrie et l'Agriculture" (IRSIA) for financial support.

[1]N. Mangelson, F. Ajzenberg-Selove, M. Reed, and C. C. Lu, Nucl. Phys. 88, 137 (1966).
[2]J. J. Kroepfl and C. P. Browne, Nucl. Phys. A108, 289 (1968).
[3]J. A. Koepke and R. E. Brown, Phys. Rev. C 16, 18 (1977).
[4]G. Paić, B. Antolković, A. Djaloeis, J. Bojowald, and C. Mayer-Böricke, Phys. Rev. C 24, 84 (1981).
[5]D. K. Scott, Nucl. Phys. A354, 375 (1981).
[6]Th. Delbar, Ph.D. thesis, University of Louvain, Louvain-La-Neuve, 1981; Th. Delbar, G. Paić, and Gh. Grégoire (unpublished).
[7]F. S. Goulding, D. A. Landis, J. Cerny, and R. H. Pehl, Nucl. Instrum. Methods 31, 1 (1964).
[8]E. Fermi, Progr. Theor. Phys. 5, 570 (1950).
[9]R. J. Slobodrian, Rep. Prog. Theor. Phys. 34, 175 (1971).
[10]R. Hagedorn, Nuovo Cimento. 15, 434 (1960).
[11]Robert L. McGrath, J. Cerny, and E. Norbeck, Phys. Rev. Lett. 19, 1442 (1967).
[12]L. M. Delves, Nucl. Phys. 20, 275 (1960); all expressions $Y(1^{(i)},1_{i+1},\ldots)$ of pages 285 and 286 should be replaced by $Y(1^{(i-1)},1_{i+1},\ldots)$.
[13]F. Cerulus, Nuovo Cimento 22, 958 (1961).
[14]F. B. Morinigo, Nucl. Phys. A127, 116 (1969); formula (40) should be corrected to read:

$$\frac{d^2\sigma}{d\Omega_b dE_b}=\frac{Cg}{(g^2+u^2+2ugz)^{1/2}}=\frac{C}{l}g$$

for

$$4v^2w^2-(l^2-v^2-w^2)^2>0\ .$$

The notation of the original article is kept except for substituting l for the denominator of the first equation.
[15]K. M. Watson, Phys. Rev. 95, 228 (1954).
[16]A. K. Jain, J. Y. Grossiord, M. Chevalier, M. Gusakow, and J. R. Pizzi, Nucl. Phys. A216, 519 (1973).
[17]F. Ajzenberg-Selove, Nucl. Phys. A320, 1 (1979).
[18]F. Ajzenberg-Selove, Nucl. Phys. A227, 1 (1974).
[19]J. R. Quinn, M. B. Epstein, S. N. Bunker, J. W. Verba, and J. R. Richardson, Nucl. Phys. A181, 440 (1972).
[20]Th. Delbar, Gh. Grégoire, J. Lega, G. Paić, and P. Wastyn, Phys. Rev. C 14, 1659 (1976).
[21]R. Vlastou, J. B. A. England, O. Karban, and S. Bavid, Nucl. Phys. A292, 29 (1977).
[22]C. Alderliesten, A. Djaloeis, J. Bojowald, C. Mayer-Böricke, G. Paić, and T. Sawada, Phys. Rev. C 18, 2001 (1978).